HHS Public Access

Author manuscript

ACS Nano. Author manuscript; available in PMC 2023 September 01.

Published in final edited form as:

ACS Nano. 2022 April 26; 16(4): 6349–6358. doi:10.1021/acsnano.2c00423.

PEGylated liposomes accumulate in the areas relevant to skin toxicities *via* passive extravasation across "leaky" endothelium

Yue Li[1,2,#], **Laren Lofchy**[1,2,#], **Guankui Wang**[1,2,3], **Hanmant Gaikwad**[1,2,3], **Mayumi Fujita**[4,5,6], **Dmitri Simberg**[1,2,3,*]

[1]Translational Bio-Nanosciences Laboratory, University of Colorado Anschutz Medical Campus, Aurora, CO, 80045, USA

[2]Department of Pharmaceutical Sciences, The Skaggs School of Pharmacy and Pharmaceutical Sciences, University of Colorado Anschutz Medical Campus, Aurora, CO, 80045, USA

[3]Colorado Center for Nanomedicine and Nanosafety, University of Colorado Anschutz Medical Campus, Aurora, CO, 80045, USA

[4]Department of Dermatology, University of Colorado Anschutz Medical Campus, Aurora, CO, 80045, USA

[5]Department of Immunology and Microbiology, University of Colorado Anschutz Medical Campus, Aurora, CO, 80045, USA

[6]Rocky Mountain Regional Veterans Affairs Medical Center, Aurora, CO, 80045, USA

Abstract

PEGylated liposome is the cornerstone platform for modern drug delivery. Unfortunately, as exemplified by PEGylated liposomal doxorubicin (aka Doxil®), altered doxorubicin pharmacokinetics causes off-target accumulation in the skin, including palms and feet, leading to severe dose-limiting toxicity. In addition to Doxil, other nanoparticles and PEGylated liposomes exhibit significant deposition in the skin, but mechanisms of accumulation are poorly understood. Using *ex vivo* imaging and *ex vivo* confocal microscopy, we show that PEGylated liposomes in mice accumulate predominantly in the areas subject to mechanical stress/pressure. Blood vessels in foot skin appear to be especially leaky, exhibiting burst-like extravasations. Using high resolution confocal microscopy and liposomes labeled with different dyes in the membrane and/or interior, two modes of extravasation were observed: 1) as intact liposomes; 2) as separated liposomal components. On the other hand, stable crosslinked iron oxide nanoworms extravasated only as intact nanoparticles. There was no colocalization between liposomes and exosomal marker CD81, excluding the role of exocytosis. Also, *in situ* perfusion of formalin-fixed foot skin with labeled liposomes revealed that the extravasation is mediated by passive, energy-independent diffusion and not by leukocyte "hitchhiking". These findings improve our understanding of extravasation pathways of nanocarriers in the areas relevant to skin pathologies, and could lead to strategies to prevent and treat liposome-induced skin toxicities.

[*]corresponding author: dmitri.simberg@cuanschutz.edu.
[#]equal contribution

Keywords

liposome; nanoparticle; Doxil; doxorubicin; skin; extravasation

Skin is the largest organ in the body with important barrier and immune functions. Many nanosized particles, including liposomes, gold and silica nanoparticles, and quantum dots accumulate in the mouse skin.[1–7] PEGylated liposomal doxorubicin (PLD, Doxil®) is widely used for cancer therapy,[8] but has serious cutaneous toxic side effects in up to 25% of patients.[4, 9] Doxil induces severe pain, ulceration and hyperpigmentation in palms and soles, hence named “hand-foot syndrome (HFS)”, or palmar-plantar erythrodysesthesia.[4, 10] HFS coincides with mechanical stress/pressure on the affected areas, including palms, soles, armpits, sacral area, inner side of knees, posterior side of elbows, buttocks, and anterior folding lines of wrists. Therefore, patients are instructed to avoid belts, jewelry, tight clothes and bandages.[11, 12] Cutaneous toxicities typically interfere with daily living activities and thus can severely impact patients’ physical, psychological, and social well-being.[13–15] The most effective management for moderate-to-severe grade HFS is interrupting treatment, modifying dosage, and discontinuing treatment, which may affect efficacy outcomes especially in the curative setting; thus, better strategies to treat skin toxicities are urgently needed.[16]

Paradoxically, while many rigorous studies were dedicated to understanding the accumulation of nano-delivery systems in tumors[17, 18] there is a paucity of knowledge on the mechanisms of nanoparticle extravasation in the skin. For instance, the explanation of Doxil toxicity in dermatological literature states that “..the hydrophilic coating of the liposomes appears to cause drug accumulation…”[16] Excellent studies of Allen and colleagues[2] on the pharmacokinetics of liposomes in mouse skin showed that in foot skin liposomes accumulate faster and over a longer period of time than in other areas, but no mechanisms of accumulation were reported. Recently, using fiber optical near infrared spectroscopy and *ex vivo* near-infrared imaging,[19] we demonstrated that long-circulating PEGylated liposomes labeled with indocarbocyanine dye DiR showed up to a 10-fold greater skin deposition than non-PEGylated liposomes. Using intravital microscopy, we subsequently studied the dynamics of accumulation of DiI-labeled PEGylated liposomes and PEGylated liposomal doxorubicin, in ventral and dorsal skin.[20] Soon after systemic injection in mice, liposomes extravasated and accumulated in the dermis, where they were detectable for at least 7 days postinjection. While these studies demonstrated that labeled liposomes are able to extravasate from skin capillaries, it is not clear how this process takes place, given that capillaries in healthy skin are known to be nonporous[21] and not readily permeable to macromolecules.[22, 23] In particular, several key questions need to be asked: 1) which skin areas are most prone to extravasation? 2) do liposomes extravasate intact? 3) do liposomes extravasate *via* passive or active process? Here we addressed these questions using *ex vivo* imaging and *ex vivo* high magnification confocal microscopy of freshly excised skin flaps. In addition to PLD, which is a small and dim nanoparticle not readily amenable to modifications, we explored a range of PEGylated liposomal formulations labeled with bright fluorescent dyes in the membrane/interior. Our studies demonstrate that liposomes accumulate most efficiently in the areas subject to mechanical

stress/pressure. The extravasation is via intact particles, and as liposomal components. On the other hand, more stable crosslinked iron oxide nanoparticles showed extravasation only as intact particles. These data improve our understanding of the mechanisms of abnormal accumulation of nano drugs in the skin, and could lead to strategies to decrease skin toxicity of nano drugs.

RESULTS AND DISCUSSION

1. Liposomes show preferential extravasation and accumulation in skin areas subject to mechanical stress/pressure

To study the accumulation of liposomes in skin areas , we first used commercially available ~90nm PLD (LipoDox®, a generic version of Doxil, Table 1). Mice were injected i.v. with 4 mg doxorubicin/kg, and histological sections from foot skin and back skin were inspected for doxorubicin fluorescence. According to fluorescence microscopy (Fig. 1A), doxorubicin accumulation and retention were much higher in the foot than in the back skin. In the foot skin, doxorubicin showed accumulation in eccrine sweat glands and ducts, hair follicles, sebaceous glands, and also in collagenous, fibroblast-rich areas of the dermis (Fig. 1A, asterisk).

To further investigate the liposomal biodistribution, including main organs and different skin areas, we used *ex vivo* imaging. While doxorubicin can be detected by *ex vivo* imaging (not shown), the hairs on the skin lead to scattering and autofluorescence; also, biodistribution in internal organs such as liver is problematic because of strong absorbance and autofluorescence in the doxorubicin wavelength. Conversely, liposomes and nanoparticles labeled with bright indocarbocyanine lipid dyes (DiR, DiD) can be readily detected in skin and other tissues.[24 19] We prepared ~150nm HSPC/Cholesterol/DSPE-PEG2000 liposomes labeled with 0.4% DiR (Fig. 1B and Table 1). *Ex vivo* imaging of freshly excised skin 4 days post-injection revealed that many areas accumulated DiR, but the areas subject to high mechanical stress/pressure, such as heels, fingers, ribs, and spine, exhibited the strongest signal (Fig. 1C, arrows). The mean fluorescence in the foot skin was higher than in the liver, lung and kidney, and was similar to the spleen, the main clearance organ (Fig. 1D). Collectively, these data suggest that liposomes preferentially accumulate in the areas subject to mechanical stress/pressure.

To further investigate the liposomal extravasation in high mechanical stress/pressure areas, we focused on the foot skin at 1h post-injection. We found that at this time point, there is a sufficient level of extravasation to enable quantification. Instead of intravital microscopy that we used previously,[20] we performed *ex vivo* confocal microscopy of freshly excised skin flaps. While this approach does not allow monitoring the real-time dynamics, it allows much better resolution in the context of intact tissue due to lack of vibrations and breathing. Furthermore, intravital imaging through the relatively thick epidermis of the feet cannot achieve the necessary penetration depth. We prepared ~130 nm HSPC/Chol/DSPE-PEG2000 liposomes labeled with 0.4% lipophilic indocarbocyanine dye DiD (Table 1) that matches the 640 nm laser of the confocal microscope. Low magnification confocal microscopy of foot skin (from the dermis side) showed efficient binding of DiD liposomes to blood vessels and extravasation (Fig. 1E). The extravasation was not equal in all areas, with the

occurrence of highly intense fluorescent “bursts” in foot pads and heels (Fig. 1E, center of the images). Extravascular fluorescence occupied 13.4% of the image area, whereas blood vessel-associated fluorescence occupied 4.9% (Fig. 1F). At higher zoom settings, discrete fluorescent dots were observed outside blood vessels (Fig. 1G). Intravenously injected PLD displayed a similar burst-like extravasation pattern in the foot skin 1h postinjection (Fig. 1H). Side-by-side comparison showed the same degree of extravasation in mice injected either with PLD or DiD-labeled HSPC/Chol/DSPE-PEG2000 liposomes (Fig. 1I). “Zoomed in” confocal images showed a diffuse mode of drug extravasation (Fig. 1J). Liposomes composed of Egg PC (EPC)/DSPE-PEG2000/DiD showed the same burst-like extravasation pattern in excised foot skin (Supplemental Fig. 1) as well as in intact walking pads of a living mouse (Supplemental Fig. 2). Since EPC-based liposomes are easier to extrude than higher transition temperature HSPC-based liposomes (further exacerbated by the presence of 0.4% lipid label), we used EPC liposomes for all subsequent experiments.

2. Liposomes extravasate as intact particles and as separated components

The data above clearly demonstrate the ability of liposomes of different compositions to extravasate in the skin. We questioned whether the extravascular fluorescence in Figs. 1G, J contains individual liposomes. The resolution of low-magnification confocal microscopy in the context of whole skin is insufficient to provide a definite answer. In an attempt to visualize extravasated liposomes, foot skin of mice injected with PLD was cryo-sectioned into 8μm sections. High-magnification (600x) confocal imaging revealed doxorubicin accumulation in dermal endothelial cells, as well as widespread extravasation and accumulation in cell nuclei (Fig. 2). While several submicron-sized, doxorubicin-positive particles were visible (Fig. 2, arrows) along with diffuse fluorescence, the presence of individual liposomes could not be verified due to the dim liposomal fluorescence against tissue background. Attempts to prepare DiD labeled liposomes loaded with doxorubicin using remote loading were unsuccessful, whereas post-labeling of LipoDox with DiD according to the previous protocols [25, 26] resulted in free DiD contamination. To reliably identify extravasated liposomes, we prepared ~130 nm EggPC/DSPE-PEG2000 liposomes that were double-labeled with two different classes of bright membrane dyes: 0.2% of indocarbocyanine lipid DiI and 0.2% of phospholipid Cy5-distearoyl phosphatidylcholine (Table 1, Cy5-DSPE, Fig. 3A–C). Phospholipid dyes are less stable than ICLs, but they are stable in liposomes in circulation for up to 48h and in tumors at 1h postinjection.[24] The dual-labeled liposomes were injected i.v, and foot skin was excised 1h postinjection and immediately cryo-sectioned. High magnification (600x) confocal microscopy (Fig. 3D) revealed extensive binding of both dyes to dermal blood vessels and extravasation as dual-labeled particles with high level of colocalization (Fig. 3E–F), with diameter less than 1 μm. Notably, we also observed extravasation and migration of diffuse DiI and Cy5-DSPE fluorescence away from blood vessels (Figs. 3D,G), suggesting disintegration of some liposomes. This disintegration did not occur in plasma, since the liposomes are stable in circulation up to 24h post-injection[24] and do not release the dye in serum. [20]Also, the diffusion was not an artifact of sample preparation, since it was also observed in freshly excised skin (Fig. 1G). We also inspected the fresh foot skin of mice injected with double-labeled liposomes at a later time point (4 days), and found that while extravasated DiI was still present outside blood vessels, Cy5-DSPE remained only in the vascular lumen

(Supplemental Fig. 3), confirming our earlier observation that phospholipid dyes undergo degradation in tissues.[24]

To further confirm that the extravasated particles are indeed intact liposomes, we prepared ~130nm EPC/cholesterol/DSPE-PEG2000 liposomes labeled with 0.4% DiD and internally with rhodamine B (Table 1, Fig. 4A). High magnification confocal microscopy showed that the majority of the liposomes contained internal rhodamine B and surface DiD, although the distribution of fluorescence was uneven (Fig. 4B–C). One hour postinjection, both DiD and rhodamine B colocalized in liposomes in plasma (Supplemental Fig. 4). High magnification confocal microscopy of foot skin histological sections showed binding of both dyes to the dermal endothelium and extravasation of double-labeled particles with size less than 1μm (Fig. 4D–E), similar to the liposomal size assessed by imaging (Fig. 4B). Also, there was a diffuse spreading of both DiD and rhodamine B away from blood vessels and the release of some rhodamine B from liposomes (Figs. 4D,G). The data unequivocally confirm that some liposomes exit skin blood vessels as intact particles, but there is also a significant disintegration of liposomes and extravasation of liposomal components.

Next, we asked if the extravasation is specific to liposomes. We prepared ~200 nm Cy3-labeled cross-linked iron oxide nanoworms (Table 1, Cy3-CLIO NWs, Fig. 5A–B) which, unlike liposomes, have a crosslinked dextran shell and do not readily disassemble in vivo.[27] DiD-labeled liposomes and Cy3-CLIO NWs were coinjected in mice, and foot skin was harvested 1h postinjection as above. High magnification confocal microscopy of histological sections showed colocalization of liposomes and nanoparticles in the dermal endothelial cells. Both DiD liposomes and Cy3-CLIO NWs extravasated as individual particles (Fig. 5C–D), of similar size (Fig. 5E). DiD also showed the diffuse extravasation mode, whereas extravascular Cy3-CLIO NWs were observed only as discrete particles (Fig. 5C). These findings confirm that solid nanoparticles are also able to extravasate, but only as intact particles.

3. Liposomal extravasation in the foot skin is a passive, energy-independent process

Previous studies, mostly in tumors, showed that more than one pathway could be responsible for the enhanced permeability of nanomedicines (Fig. 7A). Thus, vascular permeability can be mediated by: a) energy-dependent transendothelial transport,[18, 28–31] including caveolae[32] and vesiculo-vacuolar organelles; b) passive diffusion through endothelial pores/gaps (Fig. 7A, center).[33–37] Also, animal cells constantly release extracellular vesicles (EVs) as means of intercellular communication,[38, 39] and liposomes could potentially piggyback on endothelium-derived EVs for extravasation (Fig. 7A). Indeed, the liposomal lipids including ICLs are known to become incorporated in EVs *in vitro*.[40, 41] In addition, some reports showed that liposomes including PLD are taken up by blood leukocytes,[42] which could then extravasate and deliver liposomes to the skin (Fig. 7A).

First, to elucidate the role of EVs, we injected mice with ~130nm EPC/DSPE-PEG2000 liposomes labeled with 0.4% DiI (Table 1), dissected the foot skin 1h postinjection, stained cryosections for CD31 (marker of blood vessels) and tetraspanin CD81 (a marker of EVs[43]), and examined the sections with high-magnification confocal microscopy. While the endothelium was positive for both DiI and CD81, the extravasated DiI+ liposomes

showed no colocalization with CD81 (Fig. 7B–C). These data exclude the involvement of endothelium-derived EVs in the extravasation of liposomes.

Next, to distinguish between active transport and passive diffusion (Fig. 7A), and also to address the role of leukocyte trafficking, we established a “zombie” skin formalin perfusion model, similar to what was described for tumors.[18] Perfusion with formalin stops all energy-dependent transport but preserves existing gaps in the endothelium.[44] We performed *in situ* perfusion of mouse hind limbs for 15 min with formalin or PBS, followed by 1h perfusion with DiD-labeled EggPC/DSPE-PEG2000 liposomes in 1% BSA/Ringer’s lactate buffer (Fig. 8A). According to Fig. 8B-C, formalin-perfused foot skin showed efficient extravasation, comparable to that of non-fixed skin and after *in vivo* injection (Fig. 1F). Quantification of extravascular fluorescence in freshly excised foot skin (Fig. 8C) showed only a small decrease in fixed versus non-fixed skin (15.4% *vs* 18.4% area, p-value 0.05, two-tailed t-test). These data confirm that the extravasation of liposomes mostly takes place *via* an energy-independent process. The data also rule out the role of trafficking of leukocytes and binding to lipoproteins, since the perfusion was performed in the absence of leukocytes and serum.

The premise of our work was to uncover the basic mechanisms of enhanced extravasation of PEGylated liposomes in the skin, which could explain PLD accumulation toxicity. Previous studies in tumors suggested that PLD and other liposomes extravasate as intact vesicles,[45–50] but mechanism of liposomal and nanoparticle accumulation in the skin is still not clear.[51] As opposed to tumors, skin dermis is composed of loose collagen and sparse cells, allowing visualization of single extravascular nanoparticles and liposomes at high resolution. The limitation of our study was that high magnification confocal microscopy cannot accurately measure nanoparticle size less than 200 nm due to the diffraction limit, and mostly overestimates the diameter of the particles due to fluorescence halo. However, we rarely observed extravascular liposomes that were larger than 1μm. The extravasation phenomenon is passive, suggesting diffusion via vascular gaps. [36, 44]While observed for larger liposomes and nanoparticles, we speculate that this phenomenon also applies to smaller PLD. As opposed to the foot skin, our previous intravital studies in the belly skin did not find evidence of discrete liposomes,[20] suggesting that this phenomenon may be pronounced in the areas under mechanical stress/pressure. Previous work by Rakesh Jain suggested a 400nm extravasation cutoff for passage of intact liposomes across tumor vasculature.[37] Establishing the size cutoff and characterization of the vascular pores in the skin (e.g. using precisely sized beads combined with transmission electron microscopy as was done by McDonald’s seminal studies) is a major undertaking and is beyond the scope of this study. Also, we observed extravasation of separated liposomal components, including DiD and rhodamine B. The disintegration and cargo release could be dependent on liposomal formulations and loading strategies. While we found some evidence of doxorubicin release (Fig. 2), Doxil liposome is known to be more stable than the EPC liposomes used in this study.[49] Therefore, additional experiments are required to understand factors that affect the extravasation via separated liposomal components. Thus, type of membrane lipid, loading method, payload molecule, and mechanical stress could play a role in the disintegration of liposomes in skin tissue.

Treatments for liposomal skin toxicities are palliative, minimally effective, and many of them have no clear biological rationale (e.g., antiperspirants, DMSO, cold gloves, vitamin B6, urea).[13, 16, 52] While the exact mechanism of the observed leakiness is not clear, pressure/mechanical stress can trigger vascular permeability, for example, due to mast cell degranulation and subsequent histamine release.[53] Other mediators can promote vascular permeability in response to mechanical stress including bradykinin, VEGF, complement C5a, and substance P.[23, 33, 36, 44] Understanding the pharmacological triggers of abnormal skin vascular leakiness can spur rational clinical interventions to prevent toxicity. Also, understanding nanoformulation parameters that control skin extravasation can lead to strategies to prevent or reduce HFS through reformulation, or alternatively to design effective delivery to areas of skin injury.

CONCLUSIONS

The experiments demonstrated the following: 1) liposomes show enhanced extravasation in the areas of mechanical stress/pressure, e.g., walking pads and heels, often in a burst-like pattern; 2) liposomes exhibit two modes of extravasation, *via* diffusion of intact particles and individual components, which suggests that some liposomes undergo disassembly at the endothelium/dermis interface. On the other hand, solid particles extravasate intact; 3) liposomes extravasate *via* energy-independent process that does not involve leukocytes and lipoproteins. Better understanding of the cause of the abnormal skin vascular leakiness in the absence of underlying pathologies can promote the development of treatments with better biological rationale.

METHODS

Materials:

DiD (1,1’-Dioctadecyl-3,3,3’,3’-Tetramethylindotricarbocyanine, 4-chlorobenzenesulfonate salt), DiI (1,1’-Dioctadecyl-3,3,3’,3’-Tetramethylindotricarbocyanine Perchlorate) and DiR (1,1’-Dioctadecyl-3,3,3’,3’-Tetramethylindotricarbocyanine Iodide) were from Biotium (Hayward, CA, USA). Cy5-DSPE and Cy3-DSPE were synthesized as described previously.[24] All fluorescent lipids were stored at −20ºC as 4-10mM stocks in ethanol. Whatman Nucleopore Track-Etch Membranes, bovine serum albumin were from Sigma-Aldrich (St. Louis, MO, USA). Hydrogenated soy phosphatidylcholine (HSPC), cholesterol, egg phosphatidylethanolamine, DSPE-PEG2000 were from Avanti Polar Lipids (Alabaster, AL, USA) and were kept as chloroform stocks at −20ºC. Rabbit anti-mouse CD81 (Cat. 10037) was from Cell Signaling Technology (Danvers, MA, USA). Rat anti-mouse CD31 (Cat. 102402) was from BioLegend (San Diego, CA). Goat anti-rabbit Alexa 647 antibody was from ThermoFisher. Hoechst 33342 trihydrochloride trihydrate was purchased from Life Technologies (Carlsbad, CA, USA). FITC-labeled tomato lectin (Cat. FL-1171-1) was from Vector Laboratories (Burlingame, CA, USA).

Labeled liposome and nanoparticle preparation:

To prepare liposomes, lipids were mixed at the following molar ratios: EPC/DSPE-PEG2000 (94.6/5) or HSPC/Chol/DSPE-PEG2000 (56.6/38/5) with the addition of 0.4% lipid dye in

a common solvent, and liposomes were prepared by the dehydration-rehydration method as described before [24]. Liposomes were extruded by a syringe extruder (Avestin, Ottawa, Canada) through Whatman Nucleopore Track-Etch Membranes (100 nm pore size, 15 times; 57ºC for HSPC-based liposomes). For passive internal loading of liposomes, EPC/Chol/DSPE-PEG2000/DiD lipid mix (56.6/38/5/0.4) was used. Rhodamine B (Sigma) at 1 mg/ml was included in the 20mM HEPES resuspension buffer. The solution was then vortexed at 37ºC for 30 minutes, extruded though 100 nm pore size and dialyzed against PBS overnight in 20kDa Slide-A-Lyzer® cassette (ThermoFisher). Liposomes were stored at 4°C at a final concentration of 10 mM (total lipid) for a maximum period of 8 weeks before use. The size and zeta potential was measured with Zetasizer Nano (Malvern, UK). Relatively high concentration of the membrane dye (0.4%) caused larger size and broader size distribution (PDI) than PLD.

Aminated crosslinked CLIO NWs were prepared as described before [54] and labeled with 100-fold molar excess of sulfo-Cy3 NHS ester (Lumiprobe). The excess of unreacted dye was purified by dialysis, the particles were filtered through 0.2μm syringe filter and stored at 4ºC in PBS.

Animal experiments:

The University of Colorado approved the animal experiments under protocol 103913(11). To determine the distribution of liposomes in skin and organs, liposomes were injected with 50 μl of 10mM total lipid *via* tail vein. Before sacrificing, mice were preinjected with 50μl of FITC-tomato lectin (1 mg/ml) and 50μl Hoechst 33324 (2 mg/ml) to visualize the vasculature and the nuclei. Mice were sacrificed with carbon dioxide, followed by left ventricle perfusion with PBS for 10 min to remove all residual liposomes and nanoparticles.

Organ and skin ex vivo imaging:

The back, front and foot skin was dissected and placed on a slide. Lungs, liver, spleen, kidney, intestine, brain were arranged in a 24-well plate and scanned with Li-COR Odyssey (Li-COR, Lincoln, NE) at 800 nm for DiR detection. The organs were pseudo-colored with Fiji software. Mean fluorescence was determined from 8-bit TIFF images by subtracting the background, drawing a region of interest around the organs or skin, and using the “Measure” function to determine mean gray values. Such measurement is independent of the organ cross-section area. The mean gray values of non-injected organs and skin were subtracted from the measurements.

Microscopy:

Nikon Eclipse AR1HD inverted confocal microscope with 405 nm, 488 nm, 561 nm, and 640 nm excitation lasers and corresponding emission filters was used. For high magnification imaging of liposomes and nanoparticles, they were diluted in PBS, mixed with glycerol at 1:1 ratio and 2μl were placed on slide and covered with a glass cover slip. The preparations were imaged under Apo60 oil immersion objective at 2048×2048 or 1024×1024 resolution. For low-magnification skin imaging, the fresh flaps were placed on a glass slide with dermis facing the objective and imaged using Plan Apo 10x objective. Multiple random image areas were acquired at 1024×1024 resolution. Images

were quantified with Fiji using customized macros. For calculation of the percentage of area outside of blood vessels, lectin staining in 8-bit gray image stack was selected in the FITC channel, and the selection was applied to all channels. The fluorescence was manually thresholded and the percentages of binary (positive) areas inside and outside the blood vessels were calculated using the “Measure” function.

For high magnification imaging of skin histological sections, one hour post-injection mice were perfused *via* left ventricle, foot skin was quickly dissected and snap-frozen in Tissue-Tek® O.C.T. Compound (Sakura-Finetek, Torrance, CA, USA) in isopentane (ThermoFischer) cooled in liquid nitrogen. Skin was sectioned immediately with a Leica cryostat into 8 μm sections. The sections were quickly fixed with formalin, dried, mounted with 50% glycerol and covered with a coverslip. For immunostaining, the sections were blocked with 10% goat serum and stained with anti-CD81 antibody, anti-CD31 antibody and corresponding secondary antibodies. Sections were imaged with a high magnification Apo 60x oil immersion objective. For particle size analysis in high magnification images, the “Analyze Particles” function in thresholded images was used to measure particle area, which was then converted to area-weighted diameter. All the data were plotted with Prism version 9 (GraphPad, San Diego, CA).

Zombie model:

Mice were preinjected with Hoechst/FITC-lectin 1h prior to perfusion. To establish perfusion of the systemic circuit including hindlimb feet, a 25G “butterfly” catheter connected to a peristaltic pump was inserted in the left ventricle, and the right atrium was punctured. The perfusion with PBS or 10% buffered formalin was maintained at a rate of 2 mL/min for 15 min, then the buffer was switched to DiD liposomes in 1% BSA/Ringer’s lactate for 1 hour (1 mL/min; 200μM DiD, 60 ml buffer). Finally, the liposomes were flushed away for additional 5 min with PBS, and the foot skin was either excised and imaged as is, or cryosectioned into 8μm sections and imaged with high magnification objective as described above.

Supplementary Material

Refer to Web version on PubMed Central for supplementary material.

ACKNOWLEDGEMENTS

The study was supported by the following grants (DS): NIH R01CA194058 and R01AI154959, seed grant from the Associate Dean for Research, Skaggs School of Pharmacy and Pharmaceutical Sciences, and AB Nexus grant from the University of Colorado. We would like to acknowledge Dr. Chezy Barenholz for valuable advice and inspiration for the whole project, and the late Dr. Jennifer Bourne who helped us with some of the imaging studies.

REFERENCES

(1). Hwang KJ; Padki MM; Chow DD; Essien HE; Lai JY; Beaumier PL Uptake of Small Liposomes by Non-Reticuloendothelial Tissues. Biochim Biophys Acta 1987, 901, 88–96. [PubMed: 3593727]

(2). Charrois GJ; Allen TM Multiple Injections of Pegylated Liposomal Doxorubicin: Pharmacokinetics and Therapeutic Activity. J Pharmacol Exp Ther 2003, 306, 1058–1067. [PubMed: 12808004]

(3). Sykes EA; Dai Q; Tsoi KM; Hwang DM; Chan WCW Nanoparticle Exposure in Animals Can Be Visualized in the Skin and Analysed Via Skin Biopsy. Nature Communications 2014, 5,

(4). Lotem M; Hubert A; Lyass O; Goldenhersh MA; Ingber A; Peretz T; Gabizon A Skin Toxic Effects of Polyethylene Glycol-Coated Liposomal Doxorubicin. Arch Dermatol 2000, 136, 1475–1480. [PubMed: 11115157]

(5). Cai W; Shin DW; Chen K; Gheysens O; Cao Q; Wang SX; Gambhir SS; Chen X Peptide-Labeled near-Infrared Quantum Dots for Imaging Tumor Vasculature in Living Subjects. Nano Lett 2006, 6, 669–676. [PubMed: 16608262]

(6). Kumar R; Roy I; Ohulchanskky TY; Vathy LA; Bergey EJ; Sajjad M; Prasad PN In Vivo Biodistribution and Clearance Studies Using Multimodal Organically Modified Silica Nanoparticles. ACS Nano 2010, 4, 699–708. [PubMed: 20088598]

(7). Gabizon A; Price DC; Huberty J; Bresalier RS; Papahadjopoulos D Effect of Liposome Composition and Other Factors on the Targeting of Liposomes to Experimental Tumors: Biodistribution and Imaging Studies. Cancer Res 1990, 50, 6371–6378. [PubMed: 1698120]

(8). Gabizon A; Martin F Polyethylene Glycol-Coated (Pegylated) Liposomal Doxorubicin. Rationale for Use in Solid Tumours. Drugs 1997, 54 Suppl 4, 15–21.

(9). Lorusso D; Di Stefano A; Carone V; Fagotti A; Pisconti S; Scambia G Pegylated Liposomal Doxorubicin-Related Palmar-Plantar Erythrodysesthesia (‘Hand-Foot’ Syndrome). Ann Oncol 2007, 18, 1159–1164. [PubMed: 17229768]

(10). Gabizon A; Goren D; Horowitz AT; Tzemach D; Lossos A; Siegal T Long-Circulating Liposomes for Drug Delivery in Cancer Therapy: A Review of Biodistribution Studies in Tumor-Bearing Animals. Advanced Drug Delivery Reviews 1997, 24, 337–344.

(11). Childress J; Lokich J Cutaneous Hand and Foot Toxicity Associated with Cancer Chemotherapy. Am J Clin Oncol 2003, 26, 435–436.

(12). Lyass O; Uziely B; Ben-Yosef R; Tzemach D; Heshing NI; Lotem M; Brufman G; Gabizon A Correlation of Toxicity with Pharmacokinetics of Pegylated Liposomal Doxorubicin (Doxil) in Metastatic Breast Carcinoma. Cancer 2000, 89, 1037–1047. [PubMed: 10964334]

(13). von Moos R; Thuerlimann BJ; Aapro M; Rayson D; Harrold K; Sehouli J; Scotte F; Lorusso D; Dummer R; Lacouture ME; Lademann J; Hauschild A Pegylated Liposomal Doxorubicin-Associated Hand-Foot Syndrome: Recommendations of an International Panel of Experts. Eur J Cancer 2008, 44, 781–790. [PubMed: 18331788]

(14). Lassere Y; Hoff P Management of Hand-Foot Syndrome in Patients Treated with Capecitabine (Xeloda). Eur J Oncol Nurs 2004, 8 Suppl 1, S31–40. [PubMed: 15341880]

(15). Urakawa R; Tarutani M; Kubota K; Uejima E Hand Foot Syndrome Has the Strongest Impact on Qol in Skin Toxicities of Chemotherapy. J Cancer 2019, 10, 4846–4851. [PubMed: 31598155]

(16). Kwakman JJM; Elshot YS; Punt CJA; Koopman M Management of Cytotoxic Chemotherapy-Induced Hand-Foot Syndrome. Oncol Rev 2020, 14, 442. [PubMed: 32431787]

(17). Suzuki H; Bae YH Evaluation of Drug Penetration with Cationic Micelles and Their Penetration Mechanism Using an in Vitro Tumor Model. Biomaterials 2016, 98, 120–130. [PubMed: 27182814]

(18). Sindhwani S; Syed AM; Ngai J; Kingston BR; Maiorino L; Rothschild J; MacMillan P; Zhang Y; Rajesh NU; Hoang T; Wu JLY; Wilhelm S; Zilman A; Gadde S; Sulaiman A; Ouyang B; Lin Z; Wang L; Egeblad M; Chan WCW The Entry of Nanoparticles into Solid Tumours. Nat Mater 2020, 19, 566–575. [PubMed: 31932672]

(19). Griffin JI; Benchimol MJ; Simberg D Longitudinal Monitoring of Skin Accumulation of Nanocarriers and Biologicals with Fiber Optic near Infrared Fluorescence Spectroscopy (Fonirs). J Control Release 2017, 247, 167–174. [PubMed: 28069552]

(20). Griffin JI; Wang G; Smith WJ; Vu VP; Scheinman R; Stitch D; Moldovan R; Moghimi SM; Simberg D Revealing Dynamics of Accumulation of Systemically Injected Liposomes in the Skin by Intravital Microscopy. ACS Nano 2017, 11, 11584–11593. [PubMed: 29045127]

(21). Roberts WG; Palade GE Increased Microvascular Permeability and Endothelial Fenestration Induced by Vascular Endothelial Growth Factor. J Cell Sci 1995, 108 (Pt 6), 2369–2379. [PubMed: 7673356]

(22). Egawa G; Nakamizo S; Natsuaki Y; Doi H; Miyachi Y; Kabashima K Intravital Analysis of Vascular Permeability in Mice Using Two-Photon Microscopy. Scientific Reports 2013, 3, 1932. [PubMed: 23732999]

(23). Ono S; Egawa G; Kabashima K Regulation of Blood Vascular Permeability in the Skin. Inflamm Regen 2017, 37, 11. [PubMed: 29259710]

(24). Wang G; Zannikou M; Lofchy L; Li Y; Gaikwad H; Balyasnikova IV; Simberg D Liposomal Extravasation and Accumulation in Tumors as Studied by Fluorescence Microscopy and Imaging Depend on the Fluorescent Label. ACS Nano 2021,

(25). Seynhaeve AL; Hoving S; Schipper D; Vermeulen CE; de Wiel-Ambagtsheer G; van Tiel ST; Eggermont AM; Ten Hagen TL Tumor Necrosis Factor Alpha Mediates Homogeneous Distribution of Liposomes in Murine Melanoma That Contributes to a Better Tumor Response. Cancer Res 2007, 67, 9455–9462. [PubMed: 17909055]

(26). Davies Cde L; Lundstrom LM; Frengen J; Eikenes L; Bruland SO; Kaalhus O; Hjelstuen MH; Brekken C Radiation Improves the Distribution and Uptake of Liposomal Doxorubicin (Caelyx) in Human Osteosarcoma Xenografts. Cancer Res 2004, 64, 547–553. [PubMed: 14744768]

(27). Wang G; Inturi S; Serkova NJ; Merkulov S; McCrae K; Russek SE; Banda NK; Simberg D High-Relaxivity Superparamagnetic Iron Oxide Nanoworms with Decreased Immune Recognition and Long-Circulating Properties. ACS Nano 2014, 8, 12437–12449. [PubMed: 25419856]

(28). Thurston G; McLean JW; Rizen M; Baluk P; Haskell A; Murphy TJ; Hanahan D; McDonald DM Cationic Liposomes Target Angiogenic Endothelial Cells in Tumors and Chronic Inflammation in Mice. J Clin Invest 1998, 101, 1401–1413. [PubMed: 9525983]

(29). Liu X; Lin P; Perrett I; Lin J; Liao YP; Chang CH; Jiang J; Wu N; Donahue T; Wainberg Z; Nel AE; Meng H Tumor-Penetrating Peptide Enhances Transcytosis of Silicasome-Based Chemotherapy for Pancreatic Cancer. J Clin Invest 2017, 127, 2007–2018. [PubMed: 28414297]

(30). Liu Y; Huo Y; Yao L; Xu Y; Meng F; Li H; Sun K; Zhou G; Kohane DS; Tao K Transcytosis of Nanomedicine for Tumor Penetration. Nano Lett 2019, 19, 8010–8020. [PubMed: 31639306]

(31). Dvorak AM; Kohn S; Morgan ES; Fox P; Nagy JA; Dvorak HF The Vesiculo-Vacuolar Organelle (Vvo): A Distinct Endothelial Cell Structure That Provides a Transcellular Pathway for Macromolecular Extravasation. J Leukoc Biol 1996, 59, 100–115. [PubMed: 8558058]

(32). Feng Y; Venema VJ; Venema RC; Tsai N; Behzadian MA; Caldwell RB Vegf-Induced Permeability Increase Is Mediated by Caveolae. Invest Ophthalmol Vis Sci 1999, 40, 157–167. [PubMed: 9888439]

(33). Monsky WL; Fukumura D; Gohongi T; Ancukiewcz M; Weich HA; Torchilin VP; Yuan F; Jain RK Augmentation of Transvascular Transport of Macromolecules and Nanoparticles in Tumors Using Vascular Endothelial Growth Factor. Cancer Res 1999, 59, 4129–4135. [PubMed: 10463618]

(34). Belykh E; Shaffer KV; Lin C; Byvaltsev VA; Preul MC; Chen L Blood-Brain Barrier, Blood-Brain Tumor Barrier, and Fluorescence-Guided Neurosurgical Oncology: Delivering Optical Labels to Brain Tumors. Front Oncol 2020, 10, 739. [PubMed: 32582530]

(35). Hobbs SK; Monsky WL; Yuan F; Roberts WG; Griffith L; Torchilin VP; Jain RK Regulation of Transport Pathways in Tumor Vessels: Role of Tumor Type and Microenvironment. Proc Natl Acad Sci U S A 1998, 95, 4607–4612. [PubMed: 9539785]

(36). Hashizume H; Baluk P; Morikawa S; McLean JW; Thurston G; Roberge S; Jain RK; McDonald DM Openings between Defective Endothelial Cells Explain Tumor Vessel Leakiness. Am J Pathol 2000, 156, 1363–1380. [PubMed: 10751361]

(37). Yuan F; Dellian M; Fukumura D; Leunig M; Berk DA; Torchilin VP; Jain RK Vascular Permeability in a Human Tumor Xenograft: Molecular Size Dependence and Cutoff Size. Cancer Res 1995, 55, 3752–3756. [PubMed: 7641188]

(38). Budnik V; Ruiz-Canada C; Wendler F Extracellular Vesicles Round Off Communication in the Nervous System. Nat Rev Neurosci 2016, 17, 160–172. [PubMed: 26891626]

(39). Maas SLN; Breakefield XO; Weaver AM Extracellular Vesicles: Unique Intercellular Delivery Vehicles. Trends Cell Biol 2017, 27, 172–188. [PubMed: 27979573]

(40). Grange C; Tapparo M; Bruno S; Chatterjee D; Quesenberry PJ; Tetta C; Camussi G Biodistribution of Mesenchymal Stem Cell-Derived Extracellular Vesicles in a Model of Acute

Kidney Injury Monitored by Optical Imaging. Int J Mol Med 2014, 33, 1055–1063. [PubMed: 24573178]

(41). Morelli AE; Larregina AT; Shufesky WJ; Sullivan ML; Stolz DB; Papworth GD; Zahorchak AF; Logar AJ; Wang Z; Watkins SC; Falo LD Jr.; Thomson AW Endocytosis, Intracellular Sorting, and Processing of Exosomes by Dendritic Cells. Blood 2004, 104, 3257–3266. [PubMed: 15284116]

(42). Zamboni WC; Maruca LJ; Strychor S; Zamboni BA; Ramalingam S; Edwards RP; Kim J; Bang Y; Lee H; Friedland DM; Stoller RG; Belani CP; Ramanathan RK Bidirectional Pharmacodynamic Interaction between Pegylated Liposomal Ckd-602 (S-Ckd602) and Monocytes in Patients with Refractory Solid Tumors. J Liposome Res 2011, 21, 158–165. [PubMed: 20626314]

(43). Andreu Z; Yanez-Mo M Tetraspanins in Extracellular Vesicle Formation and Function. Front Immunol 2014, 5, 442. [PubMed: 25278937]

(44). Baluk P; Hirata A; Thurston G; Fujiwara T; Neal CR; Michel CC; McDonald DM Endothelial Gaps: Time Course of Formation and Closure in Inflamed Venules of Rats. Am J Physiol 1997, 272, L155–170. [PubMed: 9038915]

(45). Zhao Y; Alakhova DY; Kim JO; Bronich TK; Kabanov AV A Simple Way to Enhance Doxil(R) Therapy: Drug Release from Liposomes at the Tumor Site by Amphiphilic Block Copolymer. J Control Release 2013, 168, 61–69. [PubMed: 23474033]

(46). Schroeder A; Honen R; Turjeman K; Gabizon A; Kost J; Barenholz Y Ultrasound Triggered Release of Cisplatin from Liposomes in Murine Tumors. J Control Release 2009, 137, 63–68. [PubMed: 19303426]

(47). Silverman L; Barenholz Y In Vitro Experiments Showing Enhanced Release of Doxorubicin from Doxil(R) in the Presence of Ammonia May Explain Drug Release at Tumor Site. Nanomedicine 2015, 11, 1841–1850. [PubMed: 26115641]

(48). Zamboni WC Liposomal, Nanoparticle, and Conjugated Formulations of Anticancer Agents. Clin Cancer Res 2005, 11, 8230–8234. [PubMed: 16322279]

(49). Barenholz Y Doxil(R)--the First Fda-Approved Nano-Drug: Lessons Learned. J Control Release 2012, 160, 117–134. [PubMed: 22484195]

(50). Gabizon A; Catane R; Uziely B; Kaufman B; Safra T; Cohen R; Martin F; Huang A; Barenholz Y Prolonged Circulation Time and Enhanced Accumulation in Malignant Exudates of Doxorubicin Encapsulated in Polyethylene-Glycol Coated Liposomes. Cancer Res 1994, 54, 987–992. [PubMed: 8313389]

(51). Moghimi SM; Simberg D Nanoparticle Transport Pathways into Tumors. J Nanopart Res 2018, 20, 169. [PubMed: 29950922]

(52). Ruhstaller T; Ribi K; Sun H; Schmitz S-F; Borner M; Winkler A; Mueller A; Rohr L. v.; Winterhalder RC; Rochlitz C; Moos RV; Anchisi S; Caspar CB; Zaman K; Bodmer A; Beyeler M; Berardi S; Thurlimann BJK; Templeton A Prevention of Palmoplantar Erythrodysesthesia (Ppe) with an Antiperspirant in Breast Cancer Patients Treated with Pegylated Liposomal Doxorubicin (Pld), a Placebo-Controlled, Double Blinded, Phase Lll Trial (Sakk 92/08). Journal of Clinical Oncology 2012, 30, 9059–9059.

(53). Soter NA; Wasserman SI Physical Urticaria/Angioedema: An Experimental Model of Mast Cell Activation in Humans. J Allergy Clin Immunol 1980, 66, 358–365. [PubMed: 7002977]

(54). Wang G; Griffin JI; Inturi S; Brenneman B; Banda NK; Holers VM; Moghimi SM; Simberg D In Vitro and in Vivo Differences in Murine Third Complement Component (C3) Opsonization and Macrophage/Leukocyte Responses to Antibody-Functionalized Iron Oxide Nanoworms. Front Immunol 2017, 8, 151. [PubMed: 28239384]

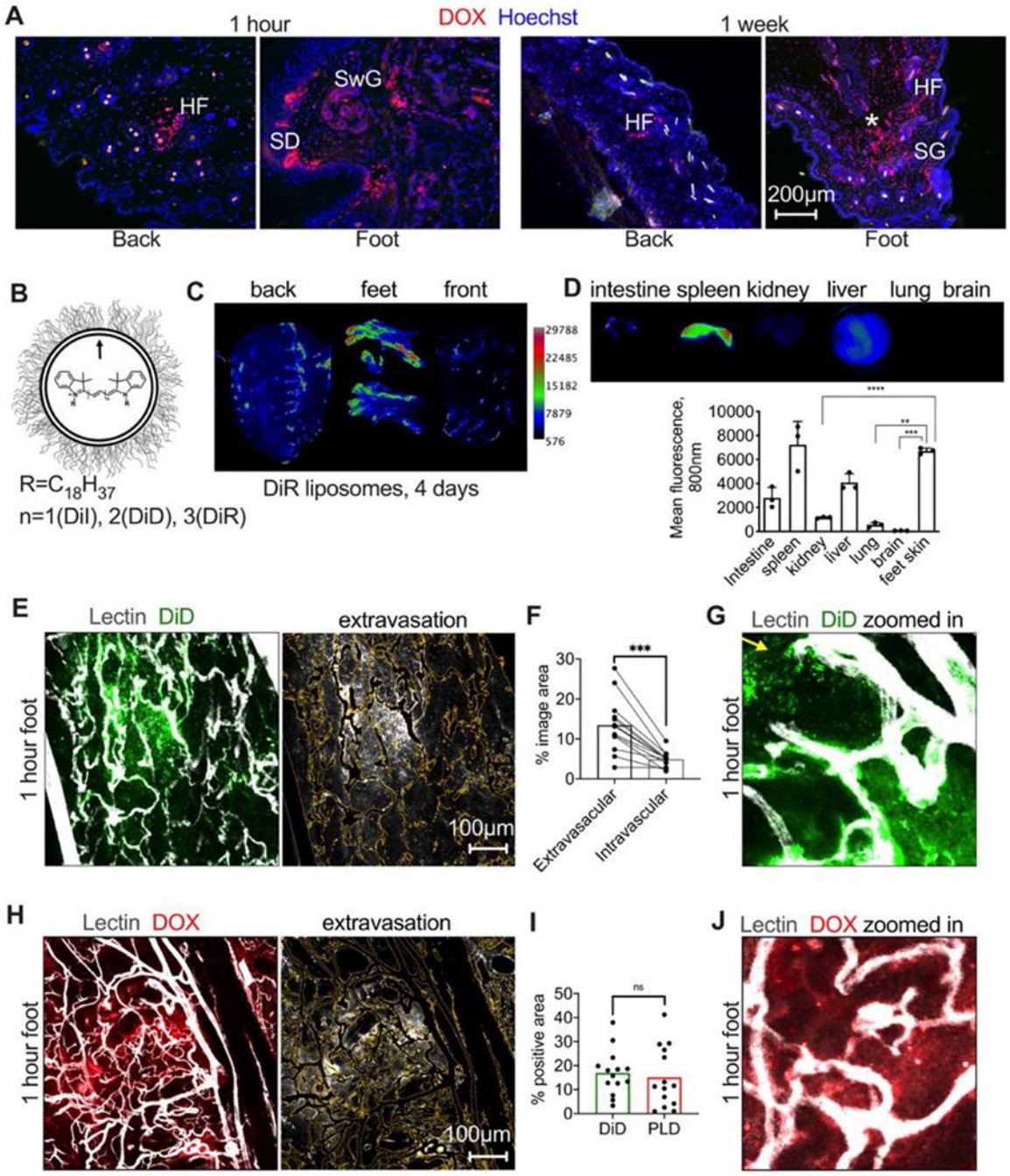

Fig. 1. Extravasation of liposomes in different skin areas.

A) Representative images of accumulation of PEGylated liposomal doxorubicin (PLD, LipoDox®) in different areas of the skin. HF, hair follicle; SD, sweat duct; SwG, sweat gland; SG, sebaceous gland; asterisk shows deep loose dermis; **B**) HSPC/Chol/DSPE-PEG2000 liposomes were labeled with indocarbocyanine dyes; **C)** pseudocolored *ex vivo* images 4 days after i.v. injection of DiR labeled liposomes show enhanced accumulation in feet and in the areas subject to mechanical stress/pressure in the back and front skin (arrows); **D**) Accumulation in the foot skin is higher than in main organs except spleen

(n=3 mice, 2 way ANOVA); **E**) mice were injected i.v with HSPC/Chol/DSPE-PEG2000 liposomes labeled with DiD, and then FITC-lectin to label blood vessels. Mice were extensively perfused with PBS to remove the blood and remaining liposomes in all experiments. Representative confocal images of excised foot skin 1h post-injection show intense “bursts” of extravasation. Image on the right shows the extravascular fluorescence after blood vessel thresholding (outlined as yellow trace); **F**) quantification of intravascular and extravascular fluorescence in multiple areas of foot skin (n=13 images, 2 feet, paired t-test); **G**) “zoomed in” area of the extravasation “burst” with discrete particles (arrow) and diffuse fluorescence; **H**) representative confocal images of excised foot skin 1h post-injection of PLD show similar burst-like extravasation (center). Image on the right shows the extravascular fluorescence after blood vessel thresholding (outlined as yellow trace); **I**) extravasation of doxorubicin fluorescence is comparable to the extravasation of PEGylated DiD liposomes (n=2 feet per group, repeated twice, two-sided t-test); **J**) representative “zoomed in” area showing doxorubicin extravasation.

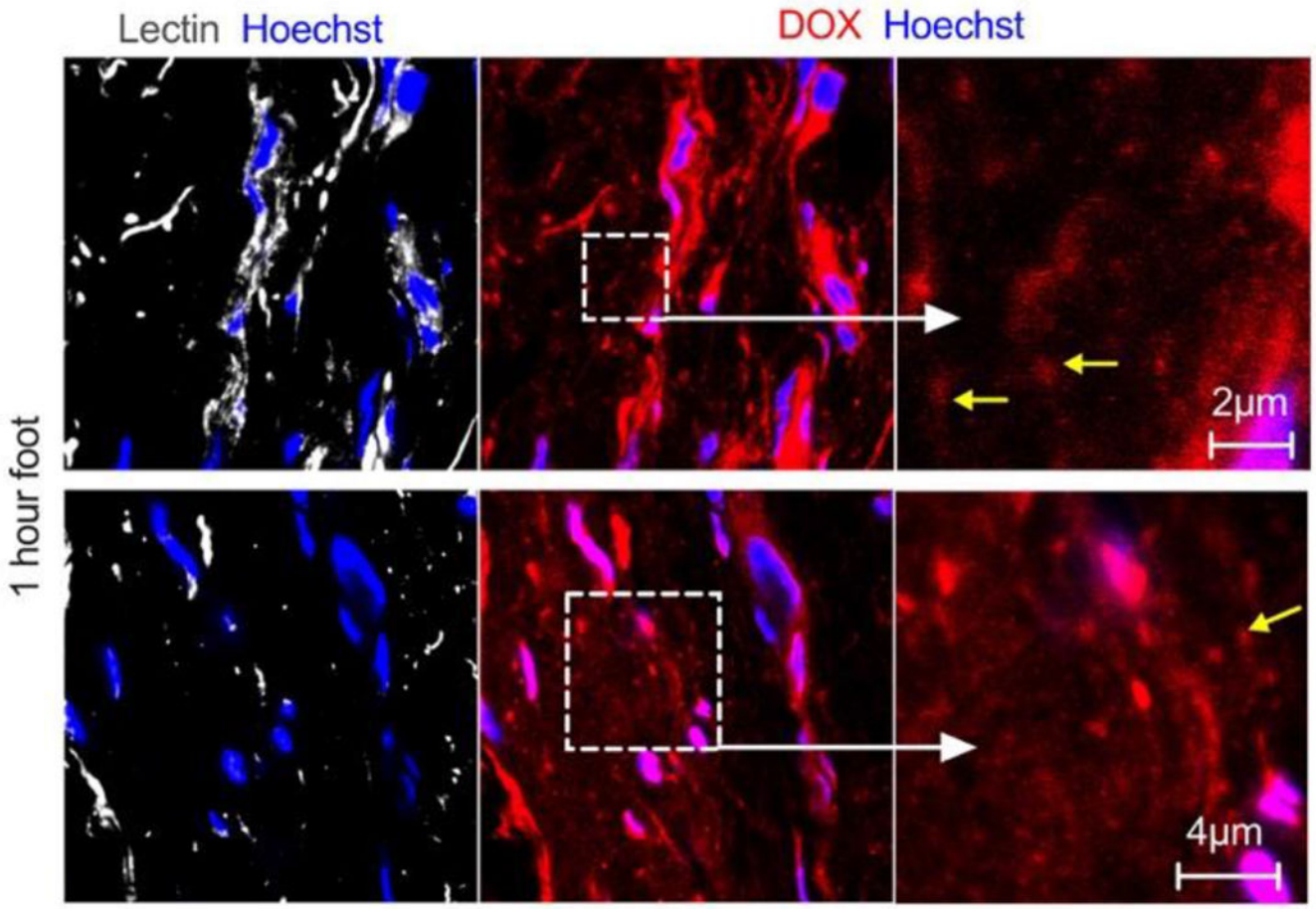

Fig 2. High-magnification microscopy of extravasation of PLD.

Representative confocal images of skin histological sections prepared 1h postinjection show accumulation of the drug in the cytoplasm and nuclei of endothelial cells and dermal cells (pink color due to overlap of both dyes), and extravasation as diffuse fluorescence. “Zoomed in” area shows endothelial staining and extravasated fluorescence. While some extravascular particles can be observed (arrows), due to dim fluorescence and small size, it is not clear if these are intact liposomes.

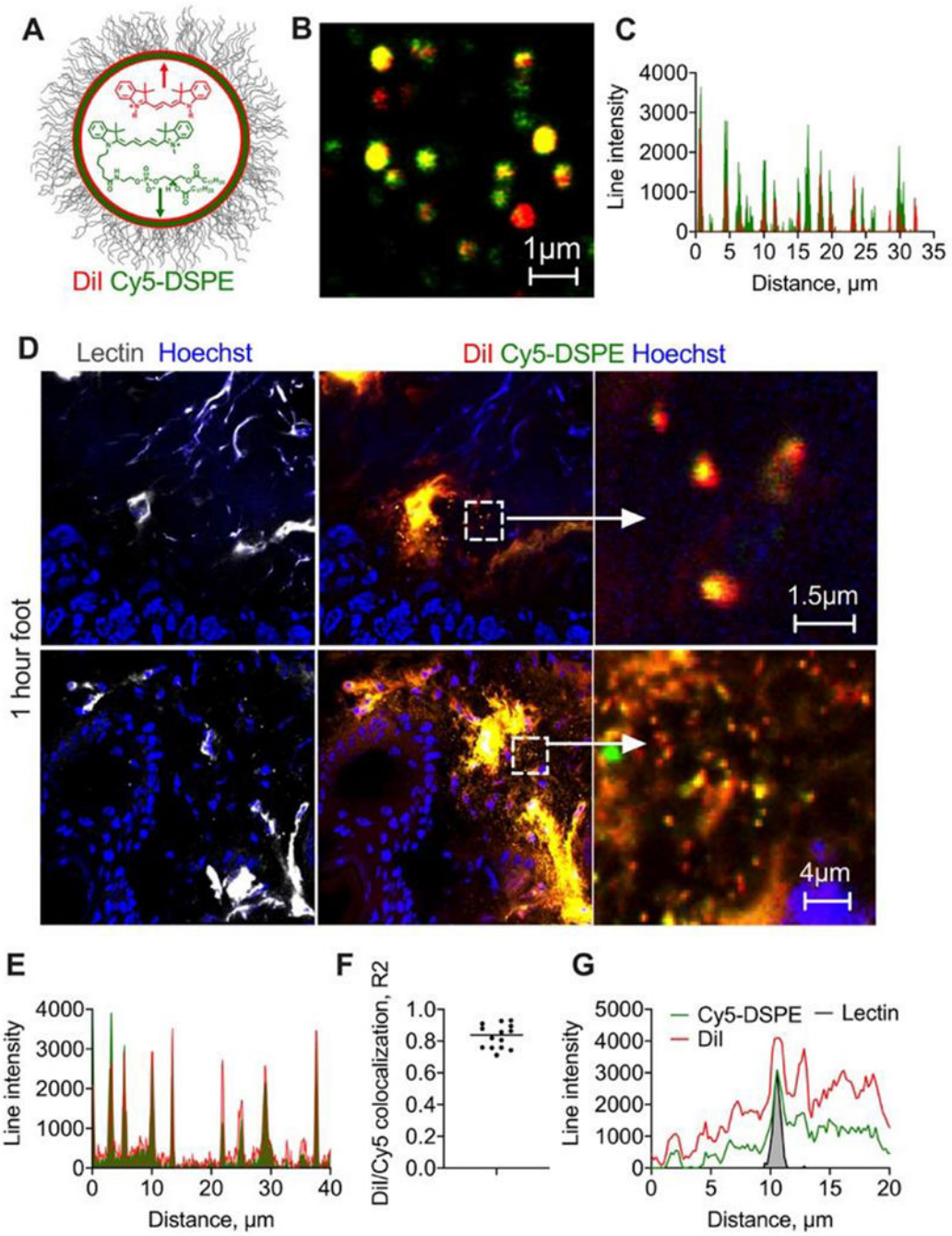

Fig. 3. Double labeled liposomes extravasate as intact particles and as diffusing lipids.

A) EggPC/DSPE-PEG2000 liposomes were labeled with lipophilic membrane dyes DiI and Cy5-DSPE; high magnification image (**B**) and line profile (**C**) show colocalization. Size is overestimated in the fluorescence images but is less than 1μm for most of the liposomes; **D**) representative confocal images of foot skin histological sections (dermis) 1h post-injection of liposomes (2 different areas). "Zoomed in" images show dual labeled extravasated particles, likely intact liposomes. Size of extravasated particles (albeit overestimated in fluorescence images) is less than 1μm; Diffusion and spreading of

both dyes away from blood vessels is also seen. Repeated in 2 mice; **E**) line profile drawn across multiple extravascular particles shows colocalization of both dyes; **F**) Person colocalization coefficient for multiple particles; **G**) representative line profile across lectin-stained endothelium shows spreading of both dyes outwards.

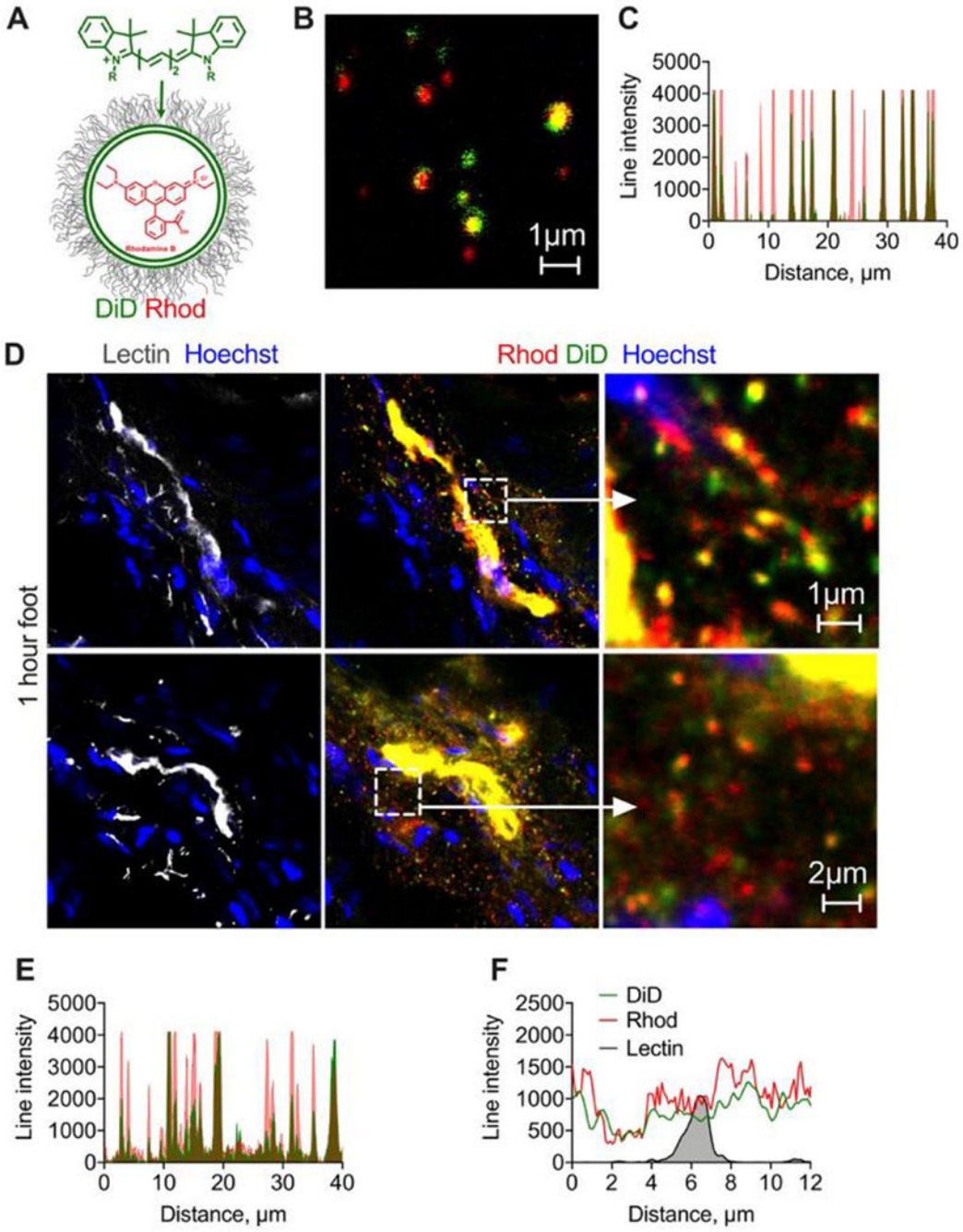

Fig. 4. Membrane- and internally-labeled liposomes extravasate as intact particles and as individual components.

A) EPC/DSPE-PEG2000 liposomes were labeled with lipophilic membrane dyes DiD and internally with rhodamine B; high magnification image (**B**) and line profile (**C**) show colocalization of both labels for the majority of liposomes, although the labels' ratio is variable. Size is overestimated in fluorescence images but is less than 1μm; **D**) representative confocal images of sections of foot skin (dermis) 1h post-injection of dual labeled liposomes (2 different areas). Cropped images show extravasated liposomes. Diameter of extravasated

particles (overestimated in fluorescence images) is less than 1μm. Diffusion of both dyes from the blood vessels can be observed. Repeated in 2 mice; **E**) line profile drawn through multiple extravasated particles shows colocalization of both dyes; **F**) representative line profile drawn across lectin+ endothelium shows spreading of both dyes. Experiment was repeated twice.

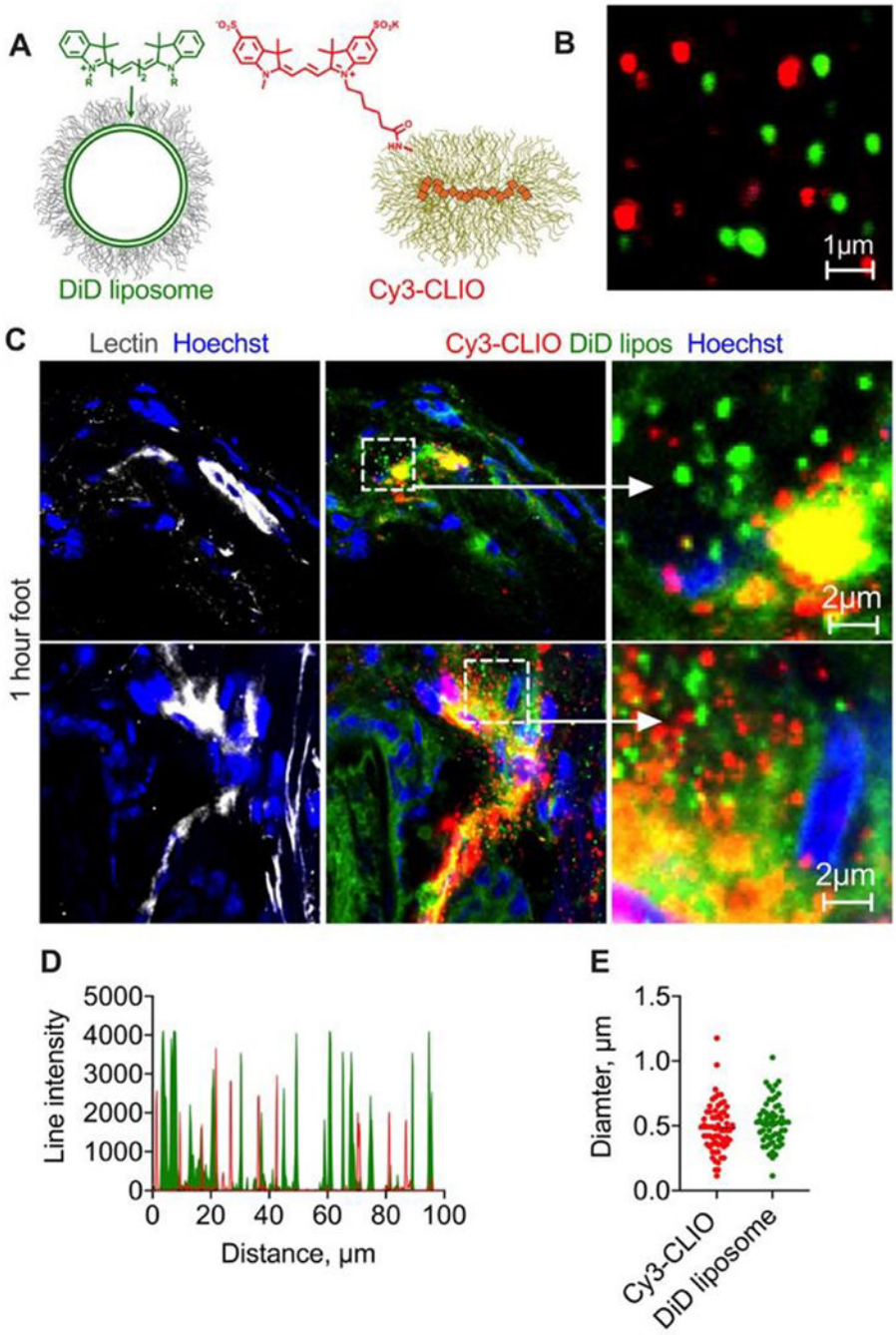

Fig. 5. Solid nanoparticles extravasate only as intact particles.

A-B) EPC/DSPE-PEG2000 liposomes labeled with DiD and similarly-sized CLIO NWs labeled with sulfo Cy3 were injected in the same mouse; **C**) representative confocal images of histological sections of foot skin (dermis) 1h post-injection of liposomes and nanoparticles (2 different areas) show that liposomes extravasated both as intact particles and as migrating DiD, whereas Cy3 extravasated only as intact particles. Repeated in 2 mice; **D**) line profile drawn though multiple extravascular particles shows almost no colocalization between Cy3-CLIO and DiD liposomes; **E**) diameter of extravasated

liposomes and nanoparticles (overestimated in fluorescence images) is similar and mostly below 1μm.

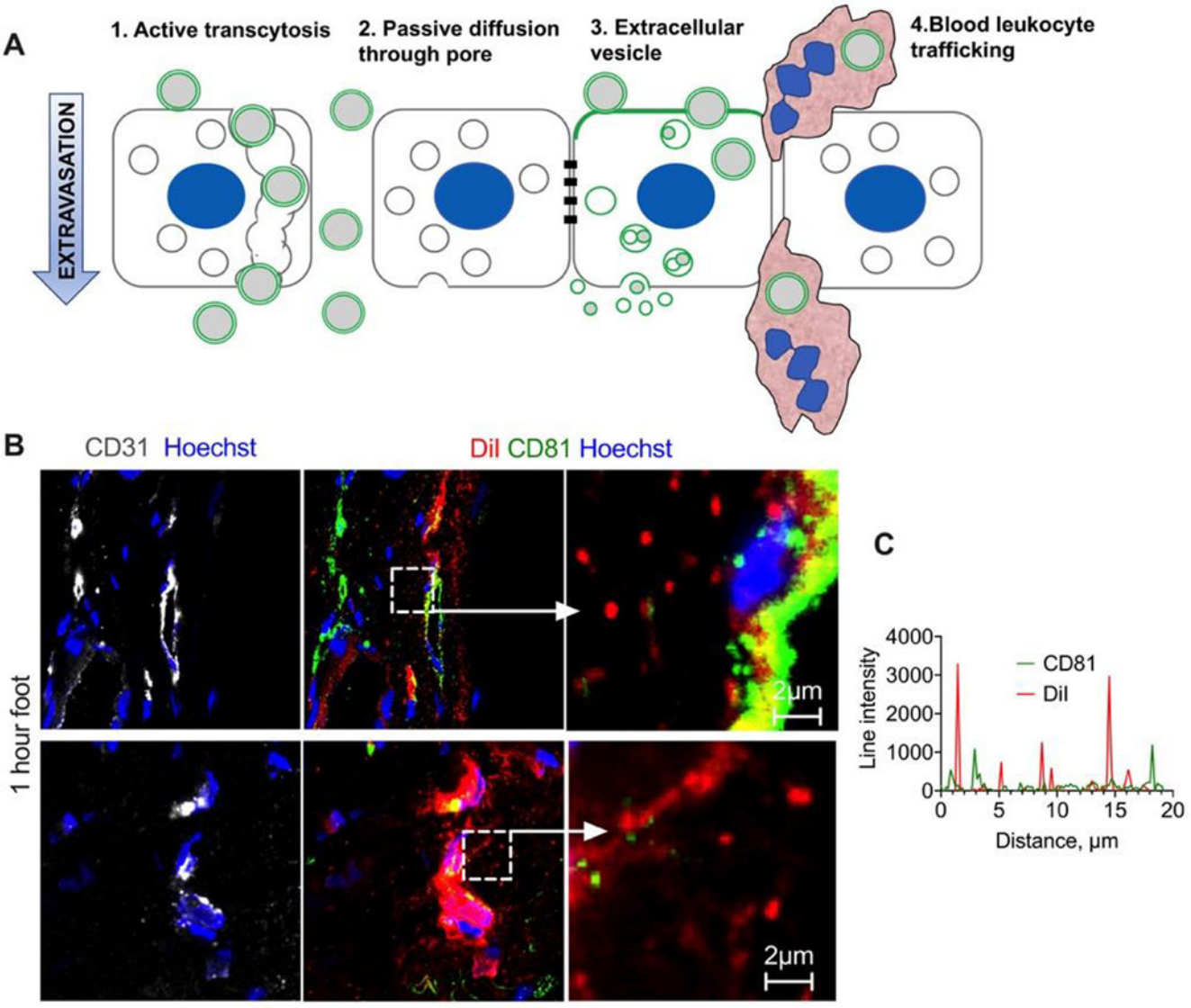

Fig. 6. Extravasation does not involve extracellular vesicle transport:

A) Possible nanomedicine extravasation pathways include active transport/transcytosis, passive diffusion *via* gaps, incorporation of liposomes in extracellular vesicle biogenesis, and leukocyte hitchhiking; **B**) Representative images of foot skin sections stained for EV marker CD81 1h post-injection of DiI labeled EPC/DSPE-PEG2000 liposomes; **C**) line profile drawn across multiple extravasated DiI+ liposomes shows almost no colocalization with CD81. Experiment repeated twice.

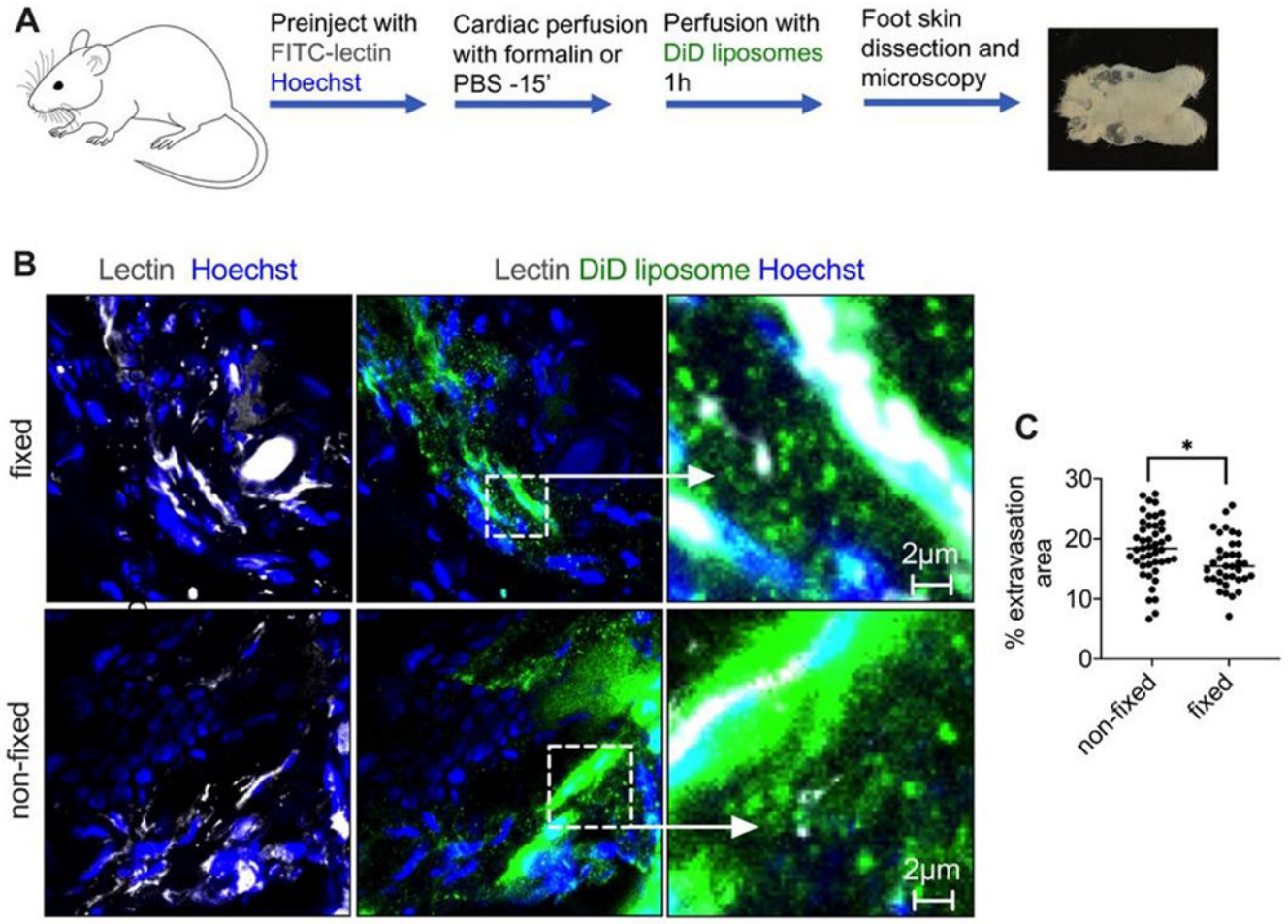

Fig. 7. Skin "zombie" model.

A) Outline of the experiment (also in Methods). Formalin-fixed or non-fixed foot skin was perfused with EPC/DSPE-PEG2000 liposomes labeled with DiD; **B**) representative high magnification images of histological sections 1h post-perfusion show extravasated intact liposomes and diffuse fluorescence in both fixed and non-fixed skin; **C**) quantification of extravascular fluorescence in multiple confocal images of intact skin (n=2 mice, 4 feet per group, repeated twice) shows only a small (p-value 0.05, two-tailed t-test) decrease in the extravasation in the fixed foot skin.

Table 1.

Characterization of the liposomes and particles with Zetasizer Nano.

Liposome and nanoparticle used in the study	Main peak, nm	PDI	ζ–potential, mV
LipoDox (HSPC/Chol/DSPE-PEG2000)	89	0.08	−28.0
HSPC/Chol/DSPE-PEG2000/DiR	155	0.2	−22.0
HSPC/Chol/DSPE-PEG2000/DiD	126	0.1	−24.0
EPC/DSPE-PEG2000/DiI/Cy5-DSPE	132	0.17	−20.1
EPC/DSPE-PEG2000/DiD	174	0.13	−13.5
EPC/DSPE-PEG2000/DiI	134	0.05	−20.0
EPC/cholesterol/DSPE-PEG2000/DiD-Rhodamine B	170	0.15	−17.8
Cy3-CLIO NW	203	0.14	+1.2
EPC/DSPE-PEG2000/DiD (large)	1613	0.4	−21.0